Searching for anomalous top quark interactions with proton tagging and timing detectors at the LHC

Cristian Baldenegro,[a] Andrea Bellora,[b] Sylvain Fichet,[c,d] Gero von Gersdorff,[e] Michael Pitt[f] and Christophe Royon[g]

[a]*Laboratoire Leprince-Ringuet, École Polytechnique,*
Rue de Fresnel 91128, Palaiseau, France

[b]*INFN Sezione di Torino and Università degli Studi di Torino,*
Via P. Giuria 1, Torino, Italy

[c]*ICTP South American Institute for Fundamental Research & IFT, UNESP,*
Rua Dr. Bento Teobaldo Ferraz 271, São Paulo, Brazil

[d]*Centro de Ciências Naturais e Humanas, Universidade Federal do ABC,*
Avenida dos Estados 5001, Santo André, Brazil

[e]*Departamento de Física, Pontifícia Universidade Católica do Rio de Janeiro,*
Rua Marquês de São Vicente 225, Rio de Janeiro, Brazil

[f]*CERN,*
CH 1211, Geneva 23, Switzerland

[g]*Department of Physics and Astronomy, The University of Kansas,*
1251 Wescoe Hall Dr, Lawrence, Kansas, U.S.A.

E-mail: c.baldenegro@cern.ch, andrea.bellora@unito.it, sfichet@caltech.edu, gersdorff@puc-rio.br, michael.pitt@cern.ch, christophe.royon@ku.edu

ABSTRACT: We study the LHC sensitivity to new broad neutral resonances produced in two-photon fusion and decaying to a top quark pair, $\gamma\gamma \to t\bar{t}$. This is probed in central exclusive $t\bar{t}$ production in proton-proton collisions, $pp \to pt\bar{t}p$. We use the tagging of the intact protons by PPS (CMS) and AFP (ATLAS) and consider the semi-leptonic $t\bar{t}$ channel. The sensitivity is also mapped onto a set of dimension-8 $\gamma\gamma t\bar{t}$ operators in the large mass limit. Using the kinematical correlations between the intact protons and the reconstructed $t\bar{t}$ system, we obtain a sensitivity to the couplings of the dimension-8 operators of $1.4 \cdot 10^{-11}\,\mathrm{GeV}^{-4}$ at 95% CL. The sensitivity to the anomalous couplings is significantly improved down to about $7 \cdot 10^{-12}\,\mathrm{GeV}^{-4}$ if the proton time-of-flight is known with a precision of 20 ps in future measurements. The 95% CL sensitivity to broad neutral resonances reaches masses of order 1500 GeV when using timing information.

Contents

1 Introduction

Under the hypothesis that new physics with strong interactions exists beyond the Standard Model (SM) of particle physics, it is possible that a new state with broad width lies at the TeV scale. Searching for such broad resonances at the LHC is somewhat challenging since the analyses cannot efficiently rely on standard bump-searching methods. Instead, the search may substantially benefit from observation channels featuring a highly reduced background. The observation channels from central exclusive production (CEP) processes, in which both protons remain intact in the final state, belong to this category and therefore provide an environment favorable to the search for broad resonances.

Among all processes, the CEP topology stands out because it can be efficiently selected using the forward proton detectors built for this purpose in the CMS and ATLAS experiments, namely the Precision Proton Spectrometer (PPS) [1] and the ATLAS Forward Proton detector (AFP) [2], respectively. Forward detectors measure the outgoing intact protons, leading to the reconstruction of the entire final state kinematics of both the proton and central systems. This set of techniques leads to drastic background reduction. A key example is the $pp \to \gamma\gamma pp$ process for which the background for $300\,\mathrm{fb}^{-1}$ drops below one

expected event in the high mass region (see e.g. [3]). It was demonstrated in [4] that this channel is an efficient precision probe of broad neutral particles.[1]

The SM central exclusive production of $t\bar{t}$ has been investigated in recent phenomenological studies [29–31]. The process has not been observed experimentally, but a recent search by the CMS Collaboration has set an upper bound on its cross section of $\sigma = 0.59$ pb at 95% CL at 13 TeV [32]. It is likely that the SM process could be observed at the high-luminosity LHC [33]. Photoproduction of top quark pairs can be used to constrain the electromagnetic dipole moments of the top quark, as discussed in ref. [34] for γ-gluon fusion processes, for example.

The goal of the present paper is to expand the prospects of CEP searches to the case of neutral particles coupled to both photons and top quarks. Our focus is on evaluating the sensitivity of the exclusive $pp \to t\bar{t}pp$ process to the presence of (possibly broad) neutral resonances. In the large mass limit the photon-top quark interactions become local and can be described using local dimension-8 effective operators. Thus, the sensitivity to these dimension-8 operators is also studied throughout this paper as a natural extension.

We emphasize that our focus on dimension-8 operators is motivated by the neutral particle scenario. In principle, searching for the dimension-6 top quark dipole operators in the CEP topology is also well-motivated. This interesting case is kept for a separate investigation. In the case of neutral particles, we will verify that the loop-generated contribution to the dipole is negligible in the scope of our study, hence justifying our focus on the dimension-8 operators.

Importantly, the sensitivity to the $pp \to t\bar{t}pp$ process is expected to be substantially enhanced by the use of timing detectors embedded into the forward detectors [35]. These timing detectors provide an independent reconstruction of the primary vertex using intact proton information, improving further the selection of signal events. Our study serves to illustrate the power of these timing detectors in the specific case of broad neutral resonances.

The plan of the paper is as follows. In section 2 the models for neutral particles are introduced. We also work out the basis of effective operators describing local $\gamma\gamma t\bar{t}$ interactions. Section 3 provides basics on forward detectors and describes the simulation framework. Section 4 briefly describes the statistical framework. Section 5 describes the search for $\gamma\gamma \to t\bar{t}$ in the semi-leptonic decay channel. Section 6 presents our results and a summary is given in section 7.

2 Effective field theory and neutral particles

Here, we define extensions of the SM which induce anomalous $\gamma\gamma \to t\bar{t}$ scattering. We start by deriving the relevant basis of higher dimensional operators that contribute to such anomalous processes. The lowest dimensional operators turn out to have dimension eight, and we identify three CP-even and three CP-odd operators. Any new physics model contributing to anomalous $t\bar{t}$ production via photon fusion can be matched to these operators at low energy. We then introduce generic models of neutral resonances with

---

trilinear couplings to both photons and top quarks. They can themselves be considered subsectors of well-motivated extensions of the SM, such as composite Higgs models, extra dimensions, etc. Moreover, we explicitly provide the matching of these generic models to the aforementioned dimension-8 effective theory. These (effective) models provide the basis for our simulations in the subsequent sections.

2.1 Operator basis

The physics candidates probed by our experiment may have a mass scale Λ much higher than the other scales involved in the amplitudes. In such a regime, the amplitudes can be expanded in inverse powers of Λ. Whenever this expansion is possible, the observable effects of the high mass physics can be described by a series of local operators encoded in a low-energy effective Lagrangian, $\mathcal{L} = \mathcal{L}_{\text{SM}} + \sum_{n,i} \frac{a_{i,n}}{\Lambda^n} \mathcal{O}_{i,n}$.

Our interest is in the set of dimension-8 operator (i.e. $n = 4$) involving two top quarks and two photons. We allow for both CP-even and CP-odd bilinear invariant in $\bar{t}t$ and photon field strength. At a given order in the expansion, the equations of motion can be used to reduce the set of the effective operators. We find an irreducible basis of six operators (omitting the subscript n),

$$
\begin{aligned}
\mathcal{O}_1 &= m_t F^{\mu\nu} F_{\mu\nu} \bar{t}t & \mathcal{O}_2 &= im_t F^{\mu\nu} \tilde{F}_{\mu\nu} \bar{t}\gamma_5 t \\
\mathcal{O}_3 &= m_t F^{\mu\nu} \tilde{F}_{\mu\nu} \bar{t}t & \mathcal{O}_4 &= im_t F^{\mu\nu} F_{\mu\nu} \bar{t}\gamma_5 t \\
\mathcal{O}_5 &= i F^{\mu\rho} F_\rho^{\ \nu} \bar{t}\gamma_\mu D_\nu t & \mathcal{O}_6 &= F^{\mu\rho} F_\rho^{\ \nu} \bar{t}\gamma_5 \gamma_\mu D_\nu t
\end{aligned}
\tag{2.1}
$$

with $\tilde{F}_{\mu\nu} = \frac{1}{2}\epsilon_{\mu\nu\rho\sigma}F^{\rho\sigma}$. The $\mathcal{O}_{1\ldots4}$ operators involve two derivatives, the $\mathcal{O}_{5,6}$ involve three derivatives. The $\mathcal{O}_{1,3,5}$ operators involve CP-even bilinear terms while $\mathcal{O}_{2,4,6}$ involve CP-odd bilinear ones.

Bilinear terms of the form $\bar{t}\Gamma\gamma_\mu\partial^\mu t$, where Γ is an arbitrary Lorentz structure, are reduced by using the top quark equation of motion into other operators from the above basis plus operators involving other fields, which are irrelevant for the process considered. One can also check that $F^{\mu\rho}\tilde{F}_\rho^{\ \nu} = \frac{1}{4}g_{\mu\nu}F\tilde{F}$ such that operators of the form $F^{\mu\rho}\tilde{F}_\rho^{\ \nu}\bar{t}\Gamma\gamma_\mu\partial_\nu t$ are reduced into $\mathcal{O}_{3,4}$ using the top quark equation of motion.

The effective Lagrangian description breaks down at momenta of order of the Λ mass scale. In case of strong coupling, this breakdown coincides with the breakdown of the perturbative expansion in the effective couplings. It also roughly coincides with violation of unitarity, signalling the necessity of a UV completion.

We parametrize the coefficients of the basis of operators shown in eq. (2.1) as

$$
\mathcal{L} = \mathcal{L}_{\text{SM}} + \sum_{i=1}^6 \zeta_i \mathcal{O}_i .
\tag{2.2}
$$

2.2 Neutral particles

Neutral particles with non-renormalizable couplings to SM operators are present in common extensions of the SM. Such theories often contain scalar, pseudo-scalar and spin-2 particles, respectively denoted by φ, $\tilde{\varphi}$ and $h^{\mu\nu}$. Examples include the Peccei-Quinn axion [36], the

Kaluza-Klein (KK) graviton and the radion in warped extra dimensions [37], the dilaton in theories of strongly coupled electroweak breaking [38], Goldstone bosons of extended composite Higgs models [39], mesons and glueballs of strongly-coupled theories [40], extra scalars breaking the global symmetry of composite Higgs models [41–43], Higgs portal models [44], and many more.

Independently of the model they originate from, their leading couplings to photons and quarks can be can be classified in terms of CP quantum numbers and written as

$$\mathcal{L}_{\text{eff}}^{\gamma\gamma} = \frac{1}{f_{\mathbf{0}_+}^{\gamma\gamma}} \varphi (F_{\mu\nu})^2 + \frac{1}{f_{\mathbf{0}_-}^{\gamma\gamma}} a F_{\mu\nu} \tilde{F}_{\mu\nu} + \frac{1}{f_{\mathbf{2}}^{\gamma\gamma}} h^{\mu\nu} \left(-F_{\mu\rho} F_\nu^\rho + \frac{1}{4} \eta_{\mu\nu} (F_{\rho\sigma})^2 \right) , \qquad (2.3)$$

$$\mathcal{L}_{\text{eff}}^{\bar{t}t} = \frac{m_t}{f_{\mathbf{0}_+}^{\bar{t}t}} \varphi \bar{t} t + i \frac{m_t}{f_{\mathbf{0}_-}^{\bar{t}t}} a \bar{t} \gamma_5 t + i \frac{1}{f_{\mathbf{2}}^{\bar{t}t}} h^{\mu\nu} \bar{t} \gamma_\mu D_\nu t \qquad (2.4)$$

where φ is the CP-even scalar, a the CP-odd scalar, and $h^{\mu\nu}$ the CP-even spin-2 field.

The couplings f_X appearing in eq. (2.3) e (2.4) are typically restricted by unitarity to satisfy

$$\frac{1}{f_X} \lesssim \frac{4\pi}{m} . \qquad (2.5)$$

Let us note that in some models that address both the hierarchy and flavor problems of the SM (such as warped extra-dimensions with SM fermions in the bulk), it is common that the heavy neutral resonances couple more strongly to the top quark than to the lighter quarks.

The partial width of both the CP-even and CP-odd scalar into $\gamma\gamma$ is

$$\Gamma_{\phi_\pm \to \gamma\gamma} = \frac{m^3}{4\pi f_{\gamma\gamma}^2} . \qquad (2.6)$$

The partial width for the CP-even and CP-odd scalar into $t\bar{t}$ are respectively

$$\Gamma_{\phi_+ \to \bar{t}t} = \frac{3}{8\pi} \frac{m_t^2}{(f_t^+)^2} m \left(1 - \frac{4m_t^2}{m^2} \right)^{3/2} \qquad (2.7)$$

$$\Gamma_{\phi_- \to \bar{t}t} = \frac{3}{8\pi} \frac{m_t^2}{(f_t^-)^2} m \left(1 - \frac{4m_t^2}{m^2} \right)^{1/2} . \qquad (2.8)$$

Matching to dimension-8 operators at tree-level. When any of these particles is heavy, it contributes to the effective EFT operators classified in eq. (2.1). The matching is as follows, depending on which of the particles is integrated out

- Spin-0, CP-even scalar ϕ

$$\zeta_1 = \frac{1}{f_{\mathbf{0}_+}^{\gamma\gamma} f_{\mathbf{0}_+}^{\bar{t}t} m^2}, \qquad \zeta_{i \neq 1} = 0 \qquad (2.9)$$

- Spin-0 CP-odd scalar $\tilde{\phi}$

$$\zeta_2 = \frac{1}{f_{\mathbf{0}_-}^{\gamma\gamma} f_{\mathbf{0}_-}^{\bar{t}t} m^2}, \qquad \zeta_{i \neq 2} = 0 \qquad (2.10)$$

- Spin-2 field $h_{\mu\nu}$

$$\zeta_1 = \frac{1}{4f_{\mathbf{2}}^{\gamma\gamma}f_{\mathbf{2}}^{t\bar{t}}m^2}, \qquad\qquad \zeta_5 = -\frac{1}{f_{\mathbf{2}}^{\gamma\gamma}f_{\mathbf{2}}^{t\bar{t}}m^2}, \qquad\qquad \zeta_{i\neq 1,5} = 0 \qquad (2.11)$$

This EFT regime typically applies in our context whenever $m \gtrsim 2.8\,\text{TeV}$ as the experimental acceptance is very low beyond this scale and a heavier resonance cannot be resolved, leaving only the imprint in the higher dimensional operators.

Estimate of dipole operator at loop-level. The above couplings of the top quark to the neutral resonance also generate a CP-even dimension-6 dipole operator

$$\zeta_d m_t F_{\mu\nu}\bar{t}\gamma^\mu\gamma^\nu\gamma^5 t \qquad (2.12)$$

where a factor of m_t arising from electroweak symmetry breaking is shown explicitly and ζ_d has a mass dimension of m^{-2}. This operator modifies the SM top quark coupling to the photon, and hence the $\gamma\gamma \to t\bar{t}$ production amplitude via the standard t-channel topology. However, the coefficient ζ_d is loop suppressed and goes as

$$\zeta_d \sim \frac{e}{16\pi^2}\frac{m_t^2}{(f^{tt})^2 m^2} \qquad (2.13)$$

and even in the strong-coupling scenario in eq. (2.5), $\zeta_d \to \frac{em_t^2}{m^4}$ suffers an additional strong $(\frac{m_t}{m})^2$ suppression. The combined effect for the modification of the SM coupling is

$$\frac{\delta e}{e} \sim \frac{m_t^3 E}{m^4} \qquad (2.14)$$

which is of the order of $\sim 10^{-6}$ for a 1 TeV resonance and a typical energy of $E = 500\,\text{GeV}$. Therefore, such an effect is completely negligible.

3 Simulation framework

3.1 Signal modeling

In our setup the anomalous $pp \to t\bar{t}pp$ process (figure 1(c)) is probed in the configuration of forward protons, i.e. in very peripheral proton-proton collisions. In very peripheral collisions, the electromagnetic field generated by the electrically charged protons can be treated as a source of quasi-real photons. These quasi-real photons can then interact to produce the top quark pair system. This photon emission off the proton is treated within the equivalent photon approximation (EPA) [45, 46]. In contrast to the standard parton distribution functions used in the quantum chromodynamics (QCD) factorization theorem, the flux and energy spectra of the quasi-real photons are under better theoretical control. This is because they are parametrized with the elastic electric and magnetic form factors extracted from precision electron-proton elastic scattering data. Due to additional soft interactions between the protons, not all of them will remain intact after the quasi-real photon exchange. This means that the cross section for photon-induced processes with
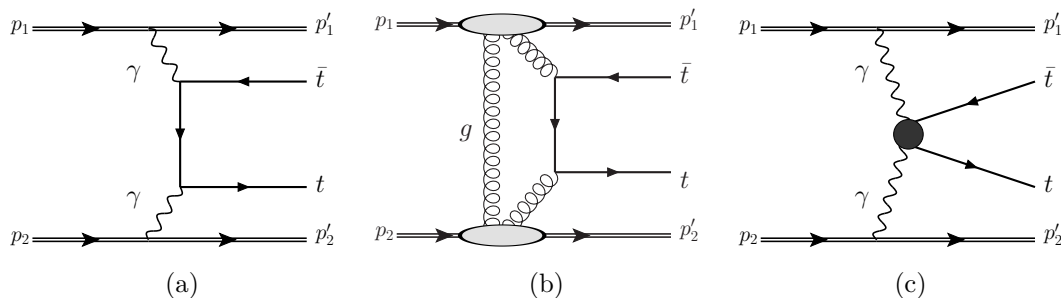
Figure 1. Feynman diagram for exclusive production of $t\bar{t}$ via photon fusion (a), color-singlet two-gluon fusion (b), and anomalous exclusive production via a local effective operator from the basis (2.1) (c).

intact protons is reduced [47–51]. For our projections, this effect is taken into account by supplementing the cross section calculation with a survival probability factor that accounts for the probability that the protons remain intact after the photon exchange. For our calculations, we assume a survival probability of 90%.

The signal process originates from the squared anomalous amplitude plus the interference with the SM exclusive production of $t\bar{t}$. The SM exclusive production of $t\bar{t}$ mainly happens via photon-initiated interaction (figure 1(a)), while the amplitude for gluon initiated CEP (figure 1(b)), which can be calculated with the perturbative QCD Durham model [47], is at least two orders of magnitude lower, thus negligible.

In the present study the SM cross section at $\sqrt{s} = 14\,\text{TeV}$, ~ 0.35 [30, 52], is between one and two orders of magnitude lower than its anomalous counterpart when considering coupling values equal to the predicted sensitivity. This difference is further enhanced when applying the selection criteria. The fact that the square SM amplitude is smaller than the square BSM amplitude necessarily implies that the latter dominates the signal while the interference is subleading (see [53]). Anticipating the final sensitivity, we can thus neglect beforehand the interference between anomalous and SM amplitudes.

The anomalous central exclusive production of $t\bar{t}$ via $\gamma\gamma$ interaction (figure 1(c)) is generated with the Forward Physics Monte Carlo (FPMC) event generator [54], which implements the EPA approach. The scattering amplitudes were computed using MadGraph [55], and implemented in FPMC.

3.2 Background modeling

The present study focuses on the reconstruction of anomalous exclusive $t\bar{t}$ production in the semi-leptonic decay channel. The dominant background components to $t\bar{t}$ exclusive production, in high-pileup conditions, are processes with final states similar to $t\bar{t}$ semi-leptonic decays, in coincidence with intact outgoing protons coming from soft diffractive pileup events. A next-to-leading order cross section of 903 pb for QCD $t\bar{t}$ production at 14 TeV with resummation at next-to-leading logarithmic accuracy is considered following ref. [56].

Soft diffractive reactions at 14 TeV are expected to have a production cross section of the order of 20 mb. During the CERN LHC Run 2, average simultaneous interactions

(pileup) in the 30-50 range were reached at the ATLAS and CMS interaction points. This high number of interactions, combined with the large soft single and central diffractive cross section yields a significant amount of forward protons coming from pileup collisions. Even if kinematic constraints between forward protons and the central system measurement can be exploited to tame this background component, as shown in the later sections, it still represents the main challenge when searching for $t\bar{t}$ exclusive production.

To take into account this effect, a conservative average number of concurrent interactions of 50 is considered. In each $t\bar{t}$ event, the number of pileup interactions is sampled from a Poisson distribution. For each pile up vertex, 0, 1 (in one detector arm) or 2 protons (in both arms) are assigned. The probability per-pileup vertex of having protons in the forward detectors is calculated using the Pythia8 event generator [57]. Then, the ξ distribution for these intact protons is sampled from a $1/\xi$ distribution, which is an approximation to the expected ξ distribution of soft diffractive interactions. The proton fractional momentum loss is considered in the range between 0.015 and 0.2 for our projections. A 2% Gaussian smearing is applied on ξ to mimic detector resolution effects.

The main background component is given by QCD $t\bar{t} + jets$ production. Simulated events for this process are generated with MadGraph and matched to parton showers and hadronization with Pythia8. A secondary background contribution is the QCD $WW + jets$ production in coincidence with pileup protons from soft diffraction. In this case the cross section considered is 131.3 pb, following ref. [58].

Another background contribution might arise from single-diffractive $t\bar{t}$ production in coincidence with pileup protons. The process cross section is expected to be $\mathcal{O}(1)$ pb. However, even though one of the intact protons might be kinematically correlated to the central system, the second pileup proton will not. Hence, it is effectively suppressed by exploiting this kinematical correlation, making it negligible.

In double-pomeron exchange, not all of the energy of each exchanged pomeron goes into the production of the $t\bar{t}$ system. This means that the invariant mass of the $t\bar{t}$ system reconstructed with the intact protons information heavily underestimates the true $t\bar{t}$ mass (see for example the diffractive mass fraction reported by CDF in [59] or figure 3 of ref. [31]). This process is therefore suppressed in the selection process.

CEP of $t\bar{t}$ by color-singlet two-gluon exchange, which is an irreducible background component, is suppressed at high $t\bar{t}$ masses. This is because the cross section needs to be supplemented with a Sudakov form factor that accounts for the probability that there is no initial-state radiation that could spoil the exclusivity of the process. The probability that there are no gluon emissions decreases rapidly with the mass of the central system, since there is more phase-space available for them. No such Sudakov form factor is present in calculations with two-photon fusion processes. This has been shown explicitly in refs. [3, 51].

3.3 Detector simulation

The detector simulation is performed with the Delphes package, tuned with the CMS datacard [60]. Detector efficiencies and energy/momentum smearings are parametrized as a function of the particle kinematics (pseudo-rapidity, transverse momentum for tracking detectors, pseudo-rapidity and energy for calorimeters) [61, 62]. Jets are clustered with

the FastJet package [63], using the anti-k_t algorithm [64] with a distance parameter $R = \sqrt{\Delta\phi^2 + \Delta y^2} = 0.5$, and transverse momentum $p_T > 20\,\text{GeV}$. b-tagging is included following ref. [65] and takes into account both the tagging efficiency and the misidentification rate. Leptons are reconstructed within the pseudo-rapidity range $|\eta| < 2.5$, and jets for $|\eta| < 5$. Missing transverse energy is computed in a particle-flow approach.

To account for the proton measurement resolution, a 2% Gaussian smearing on the proton fractional momentum loss ($\xi = (p_i - p_f)/p_i$) is applied and only protons with $0.015 < \xi < 0.20$ are considered, to match the typical forward detectors acceptance.

The longitudinal position of primary vertices is randomly sampled from a Gaussian distribution of 5 cm RMS, according to the reported CMS observations [66]. Timing detector resolution effects are included by applying Gaussian smearings on the proton time of arrival, assuming a 200 m distance of forward detectors from the interaction point. Timing resolutions of 20 and 60 ps are considered, the former, being compatible with the design scenario presented in [1], and the latter accounting for performance already achieved today.

4 Statistical framework

For our projections, we need to assume a set of observed data. As commonly done, we assume that no statistical fluctuations are present in these pseudo-data, which are usually dubbed "Asimov" data and that we denote here with a prime. As mentioned before, the integrated luminosity is chosen to be $L = 300\,\text{fb}^{-1}$, which is about the expected integrated luminosity to be taken by CT-PPS and AFP in Run-3 (in Run-2, CMS and ATLAS collected about 100 of data with forward detectors at 13 TeV).

The observed events follow a Poisson distribution and for this kind of analysis we can safely neglect the systematic uncertainties. The statistics for the events together with the prediction for the event rates sets the likelihood function needed for our analysis,

$$\mathcal{L}(\sigma) = \Pr(n'|b + \sigma L)\,, \quad \Pr(\hat{n}|n) = \frac{n^{\hat{n}} e^{-n}}{\hat{n}!} \tag{4.1}$$

where b is the expected number of events from the background. In our study, depending on the cases, b may be much larger than 1 or $O(1)$. In order to draw projected exclusion contours, we take the background-only hypothesis for the Asimov data,

$$n' = b\,. \tag{4.2}$$

Our method to obtain the projected exclusion contours is the following. We define the posterior probability density for σ as $L(\sigma)\pi(\sigma)$ where the prior is $\pi(\sigma) = 1$ if $\sigma > 0$ and 0 otherwise. The highest posterior density region at $1 - \alpha$ credibility level is solved analytically and is simply given by

$$1 - \alpha = \frac{\int_0^{\sigma_\alpha} L(\sigma)\pi(\sigma)}{\int_0^\infty L(\sigma)\pi(\sigma)} = 1 - \frac{\Gamma(1 + b, b + \sigma L)}{\Gamma(1 + b, b)}\,, \tag{4.3}$$

where $\Gamma(x, y)$ is the incomplete Gamma function. The credibility regions for different values of α amount respectively to exclusion at 2σ, 3σ, 5σ in terms of standard statistical

significance.[2] The projected sensitivity to the signal that we quote is the value of σ satisfying eq. (4.3) for a given statistical significance.

5 Anomalous $\gamma\gamma \to t\bar{t}$ in the semi-leptonic decay channel

Since each of the top quarks decays to a W boson and a b quark, events can be classified depending on the W boson decays. Events in which both W boson decays are leptonic are called *fully-leptonic*. When one W boson decay is hadronic and other is leptonic the event is called *semi-leptonic*. When two hadronic W boson decays take place, events are called *fully-hadronic*.

Fully-leptonic decays generally present lower backgrounds, but have a low branching fraction of the order of 10%, and the presence of two neutrinos in the final state lowers the precision of the $t\bar{t}$ system mass measurement, effectively reducing the background rejection provided by the measurement of the leading protons. Fully-hadronic decays on the other hand have the highest branching fraction. They are however strongly impacted by QCD jets backgrounds, so they represent a challenging environment for exclusive $t\bar{t}$ measurements. For the present study, the event selection and reconstruction was therefore tuned for semi-leptonic events, as they represent a good compromise under all the above-mentioned aspects.

Throughout this section the signal is taken to be generated from the basis of $t\bar{t}\gamma\gamma$ dimension-8 operators (see eq. (2.1)). The analysis is applied to signal events from neutral particles in the next section.

5.1 Event selection and reconstruction

Exclusive semi-leptonic $t\bar{t}$ events are selected in three steps: pre-selection, central selection and matching and eventually timing. A pre-selection is applied to select events with at least one lepton in the final state, two b-tagged jets, two non b-tagged jets, and one tagged proton per detector side. Furthermore, a missing energy transverse $E_T^{\text{miss}} > 20\,\text{GeV}$ is required.

EFT operators yield $t\bar{t}$ mass distributions that can be grouped into two families: $\mathcal{O}_5$ and $\mathcal{O}_6$, which contain an additional derivative, produce cross sections that grow faster with $m_{t\bar{t}}$, compared to $\mathcal{O}_1, \mathcal{O}_2, \mathcal{O}_3, \mathcal{O}_4$. The two families are thus studied in parallel, and $\mathcal{O}_1$ and $\mathcal{O}_5$ are shown as their representatives.

As illustrated in figure 2, anomalous $t\bar{t}$ events are expected to show mass distributions peaked towards higher values with respect to SM $t\bar{t}$. The two b-tagged jets and non b-tagged jets with the largest transverse momenta are therefore chosen, as well as the largest p_T lepton.

The mass of the central system can be expressed in relation to the proton measurement with:

$$m_{t\bar{t}}^p = \sqrt{s\xi_+\xi_-} \tag{5.1}$$

---

[2]The standard statistical significance is given by $Z_\alpha = \Phi^{-1}(1 - \alpha) = -\sqrt{2}\text{Erf}^{-1}(2\alpha - 1)$. We can also notice that for $b \gg 1$, upon approximating $\Gamma(x,y) \sim y^{x-1}e^{-y}$ and expanding in small $\frac{s}{b}$ we obtain $\frac{s_\alpha}{\sqrt{b}} = \sqrt{-2\log\alpha}$, where $s_\alpha = \sigma_\alpha L$. If $\alpha \ll 1$ we also have $Z_\alpha \approx \sqrt{-2\log\alpha}$, therefore in this limit our formula reproduces the standard relation $Z_\alpha = \frac{s_\alpha}{\sqrt{b}}(1 + O(\frac{s}{b}))$.
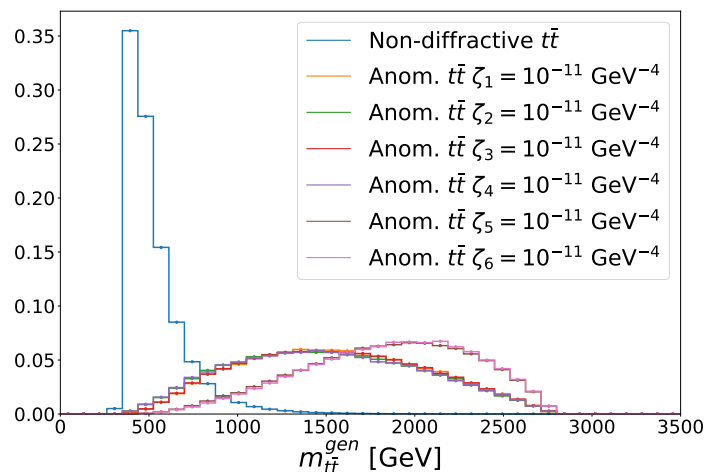
Figure 2. Mass of the $t\bar{t}$ system at generator level (stable-particle level). All histograms are normalized to unity.

with ξ_+ and ξ_- being the fractional momentum losses of the protons measured in the two proton detectors. The proton with the largest ξ is chosen to enhance the event selection efficiency of anomalous $t\bar{t}$ exclusive events in case of multiple protons on each detector side.

After the pre-selection is performed, each top quark is reconstructed from its decay product. In the following, t_h refers to the top quark that decays into hadrons, while t_ℓ refers to the one decaying into leptons.

To assign the b-tagged jets to their respective top (anti)quark, the mass of the system formed by the two non b-tagged jets and a b-tagged jet is computed. The b-jet assigned to t_h is thus the one yielding a mass measurement closest to the top quark mass. The other b-jet is consequently assigned to t_ℓ. t_ℓ is reconstructed together with the highest p_T lepton and missing transverse energy. In order to improve the t_ℓ reconstruction, the longitudinal component of the neutrino four-momentum (p_z^ν) is estimated. The value of p_z^ν is computed analytically based on the relation of the four-momentum of the lepton-neutrino system and the W boson mass,

$$\sqrt{(E^\ell + E^\nu)^2 - (\mathbf{p}^\ell + \mathbf{p}^\nu)^2} = m_W \tag{5.2}$$

where the lepton kinematics are measured, $p_T^\nu = E_T^{\mathrm{miss}}$, and the neutrino mass is neglected. The solution that minimizes $|p_z^\nu - p_z^\ell|$ is chosen, and in case of imaginary solutions only the real part is considered.

With both t_h and t_ℓ reconstructed, further selection is performed based on their kinematics. As shown by figure 3, the top quark p_T spectrum in anomalous $t\bar{t}$ exclusive production is broader with respect to the SM, and higher values are more frequent. A selection of $p_T > 425\,\mathrm{GeV}$ for both t_h and t_ℓ is therefore applied.

A similar approach is applied to $m_{t\bar{t}}$ (figure 4), the mass measured by the central detector, selecting $m_{t\bar{t}} > 960\,\mathrm{GeV}$. A mass spectrum shifted towards higher values is indeed characteristic of anomalous exclusive processes. With this mass selection, the SM CEP of $t\bar{t}$ is strongly suppressed, making the interference with BSM production negligible.
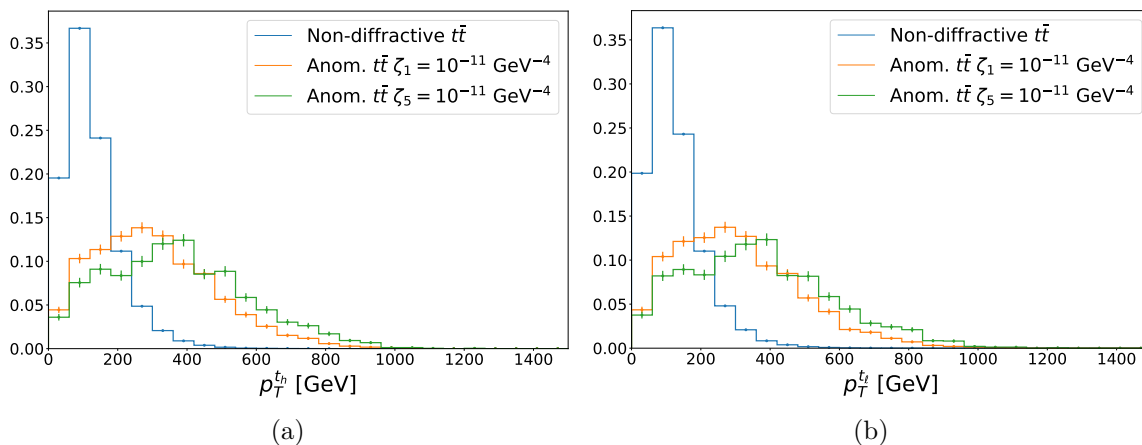
Figure 3. Transverse momentum spectrum, reconstructed from $t\bar{t}$ decay products, for the top quark decaying hadronically (a) and leptonically (b). Only events passing the pre-selection are shown. Histograms are normalized to unity.
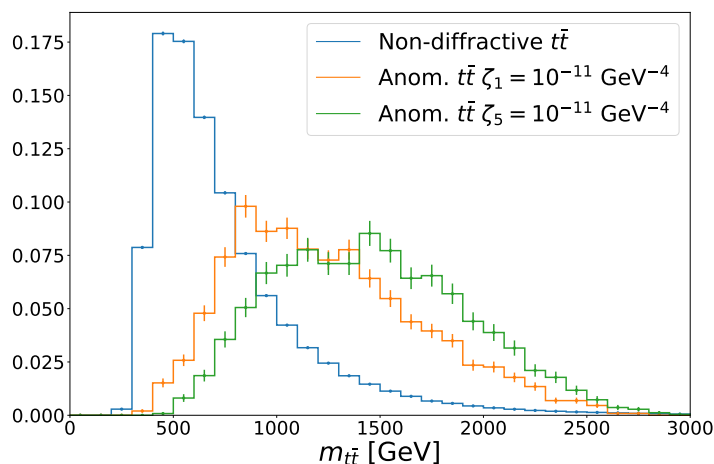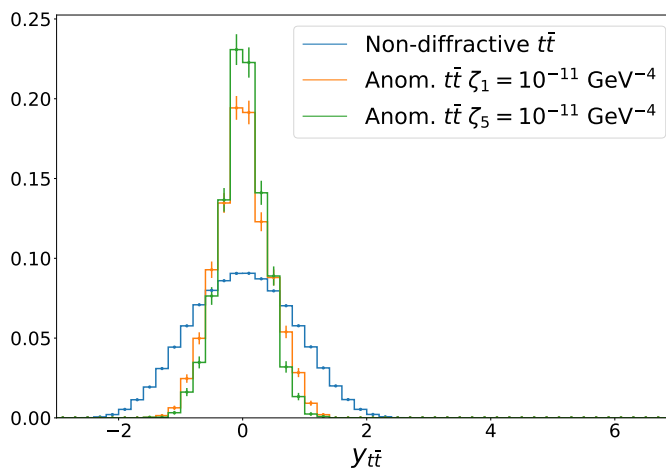

Figure 4. Invariant mass spectrum of the $t\bar{t}$ system as reconstructed from its decay products. Only events passing the pre-selection requirements are shown. Histograms are normalized to unity. The blue histogram represents the non-diffractive QCD $t\bar{t}$ component. The green and orange distributions represent the prediction of anomalous $t\bar{t}$ production assuming the coupling values of $\zeta_1 = 10^{-11}$ and $\zeta_5 = 10^{-11}\,\mathrm{GeV}^{-4}$.

Since no further radiation is expected in the final state, the tops are produced back-to-back in the transverse plane. Selecting events with acoplanarity $|1 - \frac{|\phi^{t_h} - \phi^{t_\ell}|}{\pi}| < 0.09$, as figure 5(a) illustrates, thus favors anomalous production with respect to SM $t\bar{t} + jets$ production. Further exploiting the fact that top quarks are balanced in the transverse plane, we require the ratio of their transverse momenta $p_T^{t_h}/p_T^{t_\ell} > 0.88$ (see figure 5(b)). In exclusive events, $t\bar{t}$ pairs are also produced in a narrower rapidity range (see figure 6), therefore we require $|y_{t\bar{t}}| < 0.72$.
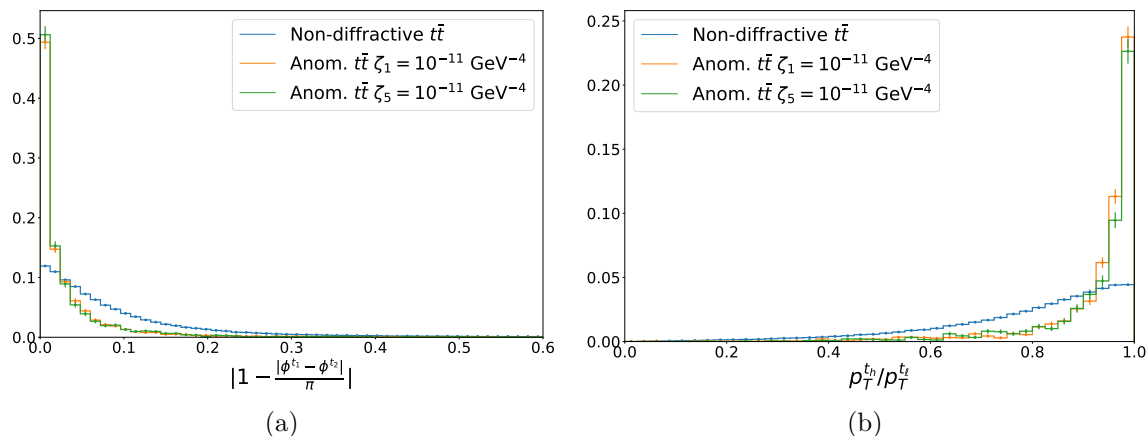
Figure 5. Acoplanarity (a) and transverse momentum balance (b), reconstructed from $t\bar{t}$ decay products. Only events passing the pre-selection are shown. Histograms are normalized to unity.
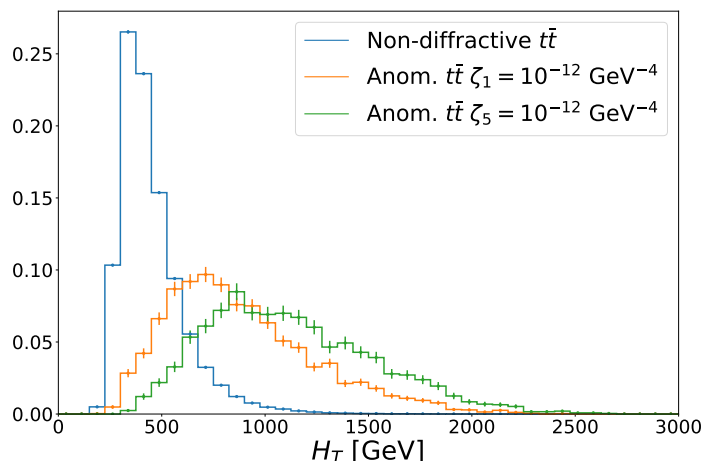

Figure 6. Rapidity distribution of the $t\bar{t}$ system as reconstructed from its decay products. Only events passing the pre-selection are shown. Histograms are normalized to unity.

Finally, a selection on the sum of the transverse momenta of the decay products H_T is performed. H_T is computed as

$$H_T = \sum_i p_T^i, \text{with } i = \ell, \nu, j_1, j_2, j_1^b, j_2^b \tag{5.3}$$

where j indicates the non b-tagged jets used for reconstruction and j^b indicates the b-tagged ones. As figure 7 shows, selecting high H_T values above 1100 GeV suppresses the SM $t\bar{t}$ background while retaining anomalous exclusive $t\bar{t}$ events.

The final selection step is performed by comparing the mass and rapidity of the final state reconstructed in the central detector from the decay products with the measurements that can be obtained from proton tagging. As shown in eq. (5.1), the mass of the central system can be measured via the fractional momentum losses of the protons. Similarly, the

Figure 7. Sum of the transverse momenta of the decay products of the $t\bar{t}$ system (H_T). Only events passing the pre-selection are shown. Histograms are normalized to unity.

rapidity of the central system can be computed from the proton kinematics:

$$y_{t\bar{t}}^p = \frac{1}{2} \log\left(\frac{\xi_+}{\xi_-}\right) \tag{5.4}$$

where ξ_+ is the fractional momentum loss of the outgoing proton with positive p_z, and ξ_- the one of the proton with negative p_z.

In background events, pileup protons are uncorrelated with the processes observed in the central system. Mass and rapidity measurements done with outgoing protons are thus expected to be uncorrelated with the same measurements given by the $t\bar{t}$ system reconstructed from its central decay products. This is reflected in variables such as the mass match ratio and $\Delta y_{t\bar{t}}$, defined as follows:

$$\frac{\Delta m_{t\bar{t}}}{m_{t\bar{t}}^p} = 1 - \frac{m_{t\bar{t}}^c}{m_{t\bar{t}}^p} \tag{5.5}$$

$$\Delta y_{t\bar{t}} = y_{t\bar{t}}^c - y_{t\bar{t}}^p \tag{5.6}$$

where the c index indicates reconstructed quantities from decay products measured in the central detector.

As figure 8 illustrates, signal events are expected to show a narrow distribution around zero, while background events form a broader one. This is due to the uncorrelated nature of the two pileup protons selected in background events. Since pileup protons follow a $1/\xi$ momentum loss distribution, the mass computed with a random combination peaks at lower values with respect to $m_{t\bar{t}}$, so negative mass match ratios are favored. Event candidates are classified as signal when $|\frac{\Delta m_{t\bar{t}}}{m_{t\bar{t}}^p}| < 0.08$ and $|\Delta y| < 0.05$.

Finally, a selection based on the proton time of arrival is applied. The longitudinal vertex position reconstructed by the central tracking detectors (z^c) is required to be compatible with the one reconstructed from timing measurements (z^p), which is computed as

$$z^p = \frac{c}{2}(t_+ - t_-) \tag{5.7}$$
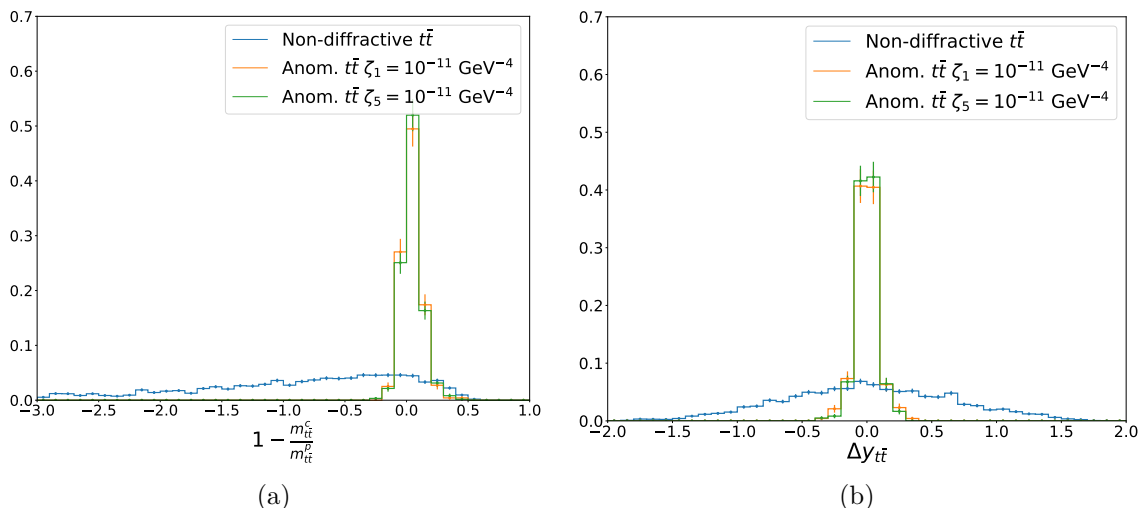
Figure 8. Mass match ratio (a) and rapidity difference (b) between the $t\bar{t}$ reconstructed from its decay products and from tagged protons. Events passing both pre-selection and central selection are shown. Histograms are normalized to unity.

Pre-selection	Central selection	Proton matching	Timing
leptons ≥ 1	$p_T^{t_h}, p_T^{t_\ell} > 425$		
b-jets ≥ 2	$m_{t\bar{t}} > 960\,\mathrm{GeV}$	$\left\|\frac{\Delta m_{t\bar{t}}}{m_{t\bar{t}}^p}\right\| < 0.08$	$\|z^p - z^c\| < 1.5\sigma$
light jets ≥ 2	$H_T > 1100\,\mathrm{GeV}$		
$E_T^{\mathrm{miss}} \geq 20\,\mathrm{GeV}$	$\|y_{t\bar{t}}\| < 0.72$	$\|\Delta y\| < 0.05$	$\left\|t_+ + t_- - \frac{2\times 200\mathrm{m}}{c}\right\| < 1.5\sigma$
protons ≥ 1 per side	$p_T^{t_h}/p_T^{t_\ell} > 0.88$		
	$\left\|1 - \frac{\|\phi^{t_h} - \phi^{t_\ell}\|}{\pi}\right\| < 0.09$		

Table 1. Summary of the analysis sequential cuts applied at each selection stage.

where c denotes the speed of light and t_+ (t_-) indicates the time of arrival of the proton with positive (negative) p_z. The distribution of $z^c - z^p$ is Gaussian in our setup, and only events falling within 1.5σ limits are accepted for maximum significance.

A similar selection is performed on the $(t_+ + t_-)$ variable, which is expected to be compatible with twice the forward detectors distance from the interaction point, divided by the speed of light, in case of protons originating from the same vertex. Also in this case, a 1.5σ compatibility requirement is applied.

A summary of the cuts applied at each selection stage is given in table 1.

Selection step	Signal		Background		
	$\zeta_1 = 5 \cdot 10^{-11}$ GeV^{-4}	$\zeta_5 = 5 \cdot 10^{-11}$ GeV^{-4}	$t\bar{t}$ (non-diffractive)	WW (non-diffractive)	CEP $t\bar{t}$ (diffractive)
Pre-selection	$2.6 \cdot 10^3$	$2.2 \cdot 10^3$	$5.0 \cdot 10^6$	$3.0 \cdot 10^3$	13
Central selection	341	487	$5.5 \cdot 10^3$	25	0
Proton matching	246	355	95	0	0
Timing (60 ps)	224	323	13.8	0	0
Timing (20 ps)	224	323	1.7	0	0

Table 2. Expected events for $300\,\text{fb}^{-1}$ at each of the selection steps, for the representatives of the operator sets $\mathcal{O}_{1\ldots4}$, $\mathcal{O}_{5\ldots6}$ and for backgrounds. All other couplings are fixed to zero. Differences among samples of the same family are within Monte Carlo statistical fluctuations.

6 Results

In this section we first display our results on the $t\bar{t}\gamma\gamma$ dimension-8 operator basis, turning on one operator at a time. We then apply the analysis to models with broad neutral resonances.

6.1 Sensitivity to dimension-8 operators

Table 2 summarizes the expected events for $300\,\text{fb}^{-1}$ for both signal and background, along the cut flow established in table 1.

The non-diffractive WW background is fully removed by the mass and rapidity matching of the central event with the proton system. The non-diffractive $t\bar{t}$ background gives ~ 100 events without the use of timing detectors. This is in contrast with the case of CEP of electroweak gauge boson pairs ($\gamma\gamma$, γZ, W^+W^-, ZZ), where the non-diffractive backgrounds can be suppressed to just a few event counts [3–5, 24]. The reason is that non-diffractive $t\bar{t}$ is dominated by gluon-initiated processes with a partonic cross section that scales with α_{s}^2, whereas non-diffractive electroweak gauge boson pair production are due to quark-initiated processes with cross sections proportional to α_{weak}^2 at leading order. Furthermore, the $t\bar{t}$ decay is significantly more challenging to reconstruct, which complicates the use of tighter event selection requirements to suppress the non-diffractive background. Using the timing detectors at the nominal resolutions of 60 ps and 20 ps, this background is reduced by a factor of ~ 7 and ~ 60.

We see that, if the timing detectors performance matches expectations, this channel may actually be a precision channel with almost no background, along the same lines as the well-known CEP $\gamma\gamma \to \gamma\gamma$ channel (see e.g. [3, 4]).

The statistical significance is computed using the expression presented in section 4, and a scan of the dimension-8 EFT operator couplings ($\zeta_{1\ldots6}$) is performed to find the 95% CL limits and the 5σ sensitivities, presented in table 3. The results are presented for three possible scenarios, considering a $300\,\text{fb}^{-1}$ integrated luminosity: without using information from timing detectors, and using them with nominal resolutions of 60 ps and 20 ps.

Coupling $[10^{-11}\,\mathrm{GeV}^{-4}]$	95% CL	5σ	95% CL (60 ps)	5σ (60 ps)	95% CL (20 ps)	5σ (20 ps)
ζ_1	1.5	2.5	1.1	1.9	0.74	1.5
ζ_2	1.4	2.4	1.0	1.7	0.70	1.4
ζ_3	1.4	2.4	1.0	1.7	0.70	1.4
ζ_4	1.5	2.5	1.0	1.8	0.73	1.4
ζ_5	1.2	2.0	0.84	1.5	0.60	1.2
ζ_6	1.3	2.2	0.92	1.6	0.66	1.3

Table 3. 95% CL and 5σ projected limits on each of the couplings, setting the other ones to zero. Multiple timing detector performance scenarios are considered: no timing information, timing detector resolution $\sigma_t = 60\,\mathrm{ps}$, and timing detector resolution $\sigma_t = 20\,\mathrm{ps}$.

6.2 Sensitivity to neutral scalars

In this section we consider a model of neutral scalar coupling to photons and top quarks (see section 2). In such a case the direct competition with other channels should be taken into account. We have verified that for any value of mass and coupling, a 5σ discovery of the neutral scalar would first occur in the $\gamma\gamma \to \gamma\gamma$ channel according to the analysis from [4]. As a result the question that should be raised is the following: in the hypothesis of a discovery of the neutral scalar in the $\gamma\gamma \to \gamma\gamma$ channel, how well could we measure the scalar's coupling to top quarks?

To answer this question, we work at the level of 95% confidence level. We assume two typical values for the coupling to the photons,

$$f_{\gamma\gamma} = \frac{m}{4\pi}, \qquad\qquad \Gamma_{\gamma\gamma} = 4\pi m \qquad\qquad \text{(Maximally broad width)} \qquad (6.1)$$

$$f_{\gamma\gamma} = \frac{m}{\sqrt{4\pi}}, \qquad\qquad \Gamma_{\gamma\gamma} = m \qquad\qquad \text{(Moderately broad width)} \qquad (6.2)$$

where we also indicate the value of the partial width into photons. For both scenarios the neutral scalar can be considered as broad since $\Gamma \geq m$. The case of maximally broad width also corresponds to the strongest coupling allowed by EFT validity or unitarity.

In figure 9 we present the projected sensitivity of our search expressed in the $pp \to t\bar{t}pp$ cross section. The CP-even and CP-odd results are very similar. We can see that in the mass range considered, the scenario with moderately broad width has better sensitivity. This is because the width from $f_{\gamma\gamma} = \frac{m}{4\pi}$ is so broad that it tends to suppress the total cross section in this mass range.

Importantly, we can see that the use of the timing detectors is key in order to increase the sensitivity of the search. Without timing detectors, the projected sensitivity in the moderately broad case goes only up to 1200 GeV and is vanishing for the maximally broad case over the considered mass range. In contrast, using the nominal performance for the timing detectors, it turns out that the sensitivity in both cases reaches $\sim 1450-1500$ GeV, a substantial improvement. In figure 10 we display the 95% CL sensitivity to the $f_{t\bar{t}}$ coupling, either with or without timing detectors. We can again see that the timing detectors are key to expand the reach of the measurement.
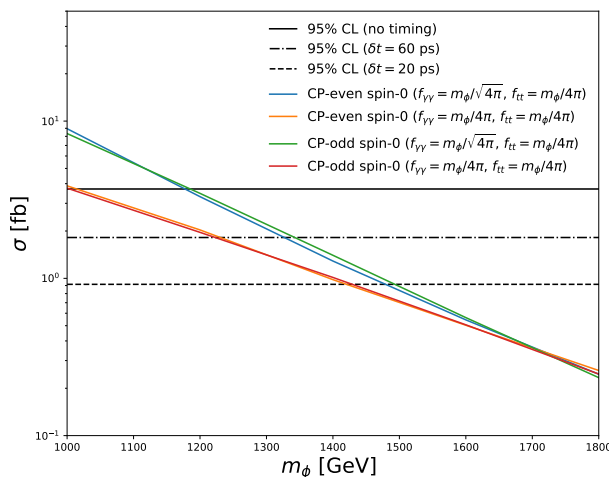
Figure 9. Projected sensitivity to the $pp \to t\bar{t}\,pp$ cross section at $95\%\,\mathrm{CL}$ as a function of the mass of the neutral scalar.
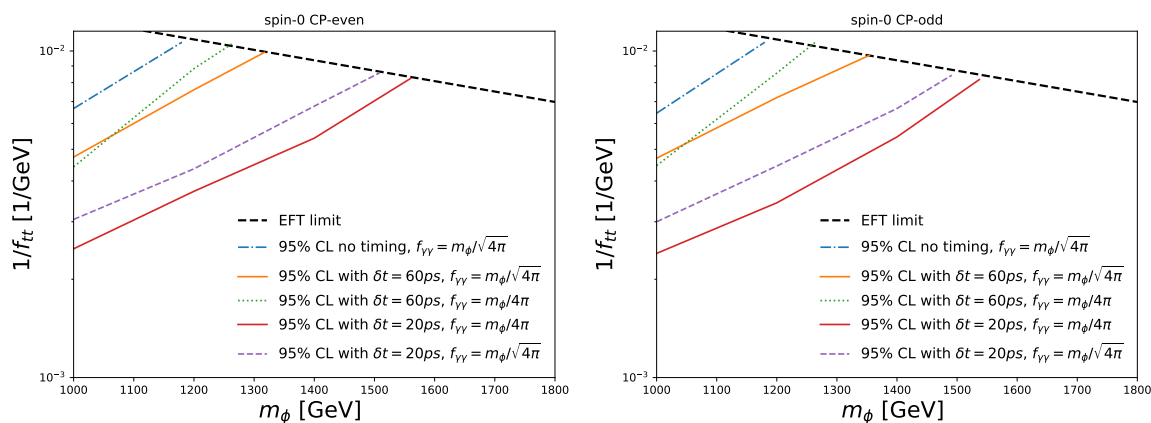
Figure 10. Projected sensitivity at $95\%\,\mathrm{CL}$ in the $(m_\phi - f_{\bar{t}t}^{-1})$ plane. Regions above the curves are sensitive to our $pp \to t\bar{t}\,pp$ search.

7 Summary and perspectives

In this work, we have studied the sensitivity of the central exclusive $pp \to pp\,t\bar{t}$ process to anomalous interactions between top quarks and photons at $\sqrt{s} = 14\,\mathrm{TeV}$. The intact protons are detected with forward proton detectors — the PPS for CMS and the AFP detector for ATLAS. We focused on the semi-leptonic decay channel of the top quark pair. We considered signals from broad neutral resonances and from $t\bar{t}\gamma\gamma$ dimension-8 local operators. Our analysis does not rely on a bump search method nor on shape analysis.

The main background for central exclusive production (CEP) processes consists of quantum chromodynamics (QCD) processes paired with forward protons from uncorrelated pileup interaction. CEP processes are efficiently selected by using the mass and rapidity of the outgoing two-proton system provided by the forward detectors. Furthermore, in the channel under consideration, it turns out that the timing detectors complementing the

forward detectors open the possibility of significant, additional background reduction. For example, at $L = 300 \, \mathrm{fb}^{-1}$, while the background with no timing information is about 100 events, the background gets reduced to $O(1)$ events when using the timing detectors with nominal resolution of 20 ps. This shows that the timing detectors have the potential to make the CEP $\gamma\gamma \to t\bar{t}$ process a high precision channel, which can be used to search for physics beyond the Standard Model.

The projected sensitivities obtained in terms of the dimension-8 operator coefficients are of order $\sim 1.5 \cdot 10^{-11} \, \mathrm{GeV}^{-4}$ (95% CL), $\sim 2.5 \cdot 10^{-11} \, \mathrm{GeV}^{-4}$ (5σ) without timing information and are of order $\sim 0.7 \cdot 10^{-11} \, \mathrm{GeV}^{-4}$ (95%CL), $\sim 1.5 \cdot 10^{-11} \, \mathrm{GeV}^{-4}$ (5σ) when using the timing detectors with nominal resolution of 20 ps.

We considered a scenario of broad neutral scalars with either moderately ($\Gamma \sim m$) or maximally ($\Gamma \sim 4\pi m$) broad width. We find that the timing information is key in order to significantly increase the sensitivity of the channel. For example for resolution of 20 ps we find 95% CL sensitivity up to mass of $\sim 1500 \, \mathrm{GeV}$, while the sensitivity is significantly worse if no timing information is used.

An extension of the present work could be to investigate hadronic decays with highly boosted topologies. The kinematics of the new physics processes considered in this study are such that boosted hadronic decays of top quarks can be reconstructed as large radii jets more frequently than in the SM. However, to fully exploit this channel, a judicious choice on jet substructure techniques needs to be taken to separate the boosted top quark topology from the overwhelming background of light-quark and gluon jets. For example, variables that are sensitive to the number of prongs in the large-radius jet, such as N-subjettiness variables, and their ratios, could be used. Also (un)groomed variables could be exploited to separate QCD top quarks, which have contributions from underlying event activity and initial-state radiation effects, from the photon-induced top quark production, which does not. We leave this as possible future work.

The present study was only focused on dimension-8 operators, as motivated by the neutral particle scenario, which generates suppressed dimension-6 operators which have been neglected here. Investigating the sensitivity of CEP $t\bar{t}$ channels to dimension-6 photon-top quark operators (namely the top quark anomalous dipoles) is an interesting direction, especially when the timing information is taken into account. This exciting possibility is left for further investigation.

Acknowledgments

References

[1] M. Albrow et al., *CMS-TOTEM Precision Proton Spectrometer*, Tech. Rep. CERN-LHCC-2014-021, TOTEM-TDR-003, CMS-TDR-13 (2014).

[2] L. Adamczyk et al., *Technical Design Report for the ATLAS Forward Proton Detector*, Tech. Rep. CERN-LHCC-2015-009, CERN-LHCC-2015-009ATLAS-TDR-024 (2015).

[3] S. Fichet, G. von Gersdorff, B. Lenzi, C. Royon and M. Saimpert, *Light-by-light scattering with intact protons at the LHC: from Standard Model to New Physics*, *JHEP* **02** (2015) 165 [arXiv:1411.6629] [InSPIRE].

[4] C. Baldenegro, S. Fichet, G. von Gersdorff and C. Royon, *Searching for axion-like particles with proton tagging at the LHC*, *JHEP* **06** (2018) 131 [arXiv:1803.10835] [InSPIRE].

[5] E. Chapon, C. Royon and O. Kepka, *Anomalous quartic $WW\gamma\gamma$, $ZZ\gamma\gamma$, and trilinear $WW\gamma$ couplings in two-photon processes at high luminosity at the LHC*, *Phys. Rev. D* **81** (2010) 074003 [arXiv:0912.5161] [InSPIRE].

[6] O. Kepka and C. Royon, *Anomalous $WW\gamma$ coupling in photon-induced processes using forward detectors at the LHC*, *Phys. Rev. D* **78** (2008) 073005 [arXiv:0808.0322] [InSPIRE].

[7] I. Sahin and S.C. Inan, *Probe of unparticles at the LHC in exclusive two lepton and two photon production via photon-photon fusion*, *JHEP* **09** (2009) 069 [arXiv:0907.3290] [InSPIRE].

[8] S. Atag, S.C. Inan and I. Sahin, *Extra dimensions in $\gamma\gamma \to \gamma\gamma$ process at the CERN-LHC*, *JHEP* **09** (2010) 042 [arXiv:1005.4792] [InSPIRE].

[9] R.S. Gupta, *Probing Quartic Neutral Gauge Boson Couplings using diffractive photon fusion at the LHC*, *Phys. Rev. D* **85** (2012) 014006 [arXiv:1111.3354] [InSPIRE].

[10] L.N. Epele, H. Fanchiotti, C.A.G. Canal, V.A. Mitsou and V. Vento, *Looking for magnetic monopoles at LHC with diphoton events*, *Eur. Phys. J. Plus* **127** (2012) 60 [arXiv:1205.6120] [InSPIRE].

[11] P. Lebiedowicz, R. Pasechnik and A. Szczurek, *Search for technipions in exclusive production of diphotons with large invariant masses at the LHC*, *Nucl. Phys. B* **881** (2014) 288 [arXiv:1309.7300] [InSPIRE].

[12] S. Fichet and G. von Gersdorff, *Anomalous gauge couplings from composite Higgs and warped extra dimensions*, *JHEP* **03** (2014) 102 [arXiv:1311.6815] [InSPIRE].

[13] S. Fichet, G. von Gersdorff, O. Kepka, B. Lenzi, C. Royon and M. Saimpert, *Probing new physics in diphoton production with proton tagging at the Large Hadron Collider*, *Phys. Rev. D* **89** (2014) 114004 [arXiv:1312.5153] [InSPIRE].

[14] H. Sun, *Probe anomalous $tq\gamma$ couplings through single top photoproduction at the LHC*, *Nucl. Phys. B* **886** (2014) 691 [arXiv:1402.1817] [InSPIRE].

[15] H. Sun, *Large Extra Dimension effects through Light-by-Light Scattering at the CERN LHC*, *Eur. Phys. J. C* **74** (2014) 2977 [arXiv:1406.3897] [InSPIRE].

[16] H. Sun, *Dark matter searches in jet plus missing energy events in γp collisions at the CERN LHC*, *Phys. Rev. D* **90** (2014) 035018 [arXiv:1407.5356] [InSPIRE].

[17] İ. Şahin et al., *Graviton production through photon-quark scattering at the LHC*, *Phys. Rev. D* **91** (2015) 035017 [arXiv:1409.1796] [InSPIRE].

[18] S.C. İnan, *Dimension-six anomalous $tq\gamma$ couplings in $\gamma\gamma$ collision at the LHC*, *Nucl. Phys. B* **897** (2015) 289 [arXiv:1410.3609] [InSPIRE].

[19] S. Fichet, *Prospects for new physics searches at the LHC in the forward proton mode*, *Acta Phys. Polon. Supp.* **8** (2015) 811 [arXiv:1510.01004] [ɪɴSPIRE].

[20] G.-C. Cho, T. Kono, K. Mawatari and K. Yamashita, *Search for Kaluza-Klein gravitons in extra dimension models via forward detectors at the LHC*, *Phys. Rev. D* **91** (2015) 115015 [arXiv:1503.05678] [ɪɴSPIRE].

[21] S. Fichet, *Shining Light on Polarizable Dark Particles*, *JHEP* **04** (2017) 088 [arXiv:1609.01762] [ɪɴSPIRE].

[22] S. Fichet, G. von Gersdorff and C. Royon, *Scattering light by light at 750 GeV at the LHC*, *Phys. Rev. D* **93** (2016) 075031 [arXiv:1512.05751] [ɪɴSPIRE].

[23] S. Fichet, G. von Gersdorff and C. Royon, *Measuring the Diphoton Coupling of a 750 GeV Resonance*, *Phys. Rev. Lett.* **116** (2016) 231801 [arXiv:1601.01712] [ɪɴSPIRE].

[24] C. Baldenegro, S. Fichet, G. von Gersdorff and C. Royon, *Probing the anomalous $\gamma\gamma\gamma Z$ coupling at the LHC with proton tagging*, *JHEP* **06** (2017) 142 [arXiv:1703.10600] [ɪɴSPIRE].

[25] S. Fichet and C. Baldenegro, *Anomalous gauge interactions in photon collisions at the LHC and the FCC*, *CERN Proc.* **1** (2018) 77 [arXiv:1708.07531] [ɪɴSPIRE].

[26] A. Senol and M. Köksal, *Analysis of anomalous quartic $WWZ\gamma$ couplings in γp collision at the LHC*, *Phys. Lett. B* **742** (2015) 143 [arXiv:1410.3648] [ɪɴSPIRE].

[27] A. Senol, *Anomalous quartic $WW\gamma\gamma$ and $ZZ\gamma\gamma$ couplings in γp collision at the LHC*, *Int. J. Mod. Phys. A* **29** (2014) 1450148 [arXiv:1311.1370] [ɪɴSPIRE].

[28] A. Senol, *$ZZ\gamma$ and $Z\gamma\gamma$ anomalous couplings in γp collision at the LHC*, *Phys. Rev. D* **87** (2013) 073003 [arXiv:1301.6914] [ɪɴSPIRE].

[29] M. Łuszczak, L. Forthomme, W. Schäfer and A. Szczurek, *Production of $t\bar{t}$ pairs via $\gamma\gamma$ fusion with photon transverse momenta and proton dissociation*, *JHEP* **02** (2019) 100 [arXiv:1810.12432] [ɪɴSPIRE].

[30] V.P. Gonçalves, D.E. Martins, M.S. Rangel and M. Tasevsky, *Top quark pair production in the exclusive processes at the LHC*, *Phys. Rev. D* **102** (2020) 074014 [arXiv:2007.04565] [ɪɴSPIRE].

[31] D.E. Martins, M. Tasevsky and V.P. Goncalves, *Challenging exclusive top quark pair production at low and high luminosity LHC*, *Phys. Rev. D* **105** (2022) 114002 [arXiv:2202.01257] [ɪɴSPIRE].

[32] CMS and TOTEM collaborations, *Search for central exclusive production of top quark pairs in proton-proton collisions at $\sqrt{s} = 13$ TeV with tagged protons*, Tech. Rep. CMS-PAS-TOP-21-007, TOTEM-NOTE-2022-002, CERN, Geneva (2022).

[33] CMS collaboration, *The CMS Precision Proton Spectrometer at the HL-LHC — Expression of Interest*, arXiv:2103.02752 [ɪɴSPIRE].

[34] M. Koksal, *Probing the anomalous electromagnetic dipole moments of the top quark in γp collision at the LHC, the HL-LHC and the HE-LHC*, *Nucl. Phys. B* **950** (2020) 114825 [arXiv:1906.09287] [ɪɴSPIRE].

[35] K. Černý, T. Sýkora, M. Taševský and R. Žlebčík, *Performance studies of Time-of-Flight detectors at LHC*, 2021 *JINST* **16** P01030 [arXiv:2010.00237] [ɪɴSPIRE].

[36] R.D. Peccei and H.R. Quinn, *CP Conservation in the Presence of Instantons*, *Phys. Rev. Lett.* **38** (1977) 1440 [ɪɴSPIRE].

[37] L. Randall and R. Sundrum, *A Large mass hierarchy from a small extra dimension*, *Phys. Rev. Lett.* **83** (1999) 3370 [`hep-ph/9905221`] [INSPIRE].

[38] W.D. Goldberger, B. Grinstein and W. Skiba, *Distinguishing the Higgs boson from the dilaton at the Large Hadron Collider*, *Phys. Rev. Lett.* **100** (2008) 111802 [`arXiv:0708.1463`] [INSPIRE].

[39] D.B. Kaplan, H. Georgi and S. Dimopoulos, *Composite Higgs Scalars*, *Phys. Lett. B* **136** (1984) 187 [INSPIRE].

[40] C.T. Hill and E.H. Simmons, *Strong Dynamics and Electroweak Symmetry Breaking*, *Phys. Rept.* **381** (2003) 235 [*Erratum ibid.* **390** (2004) 553] [`hep-ph/0203079`] [INSPIRE].

[41] G. von Gersdorff, E. Pontón and R. Rosenfeld, *The Dynamical Composite Higgs*, *JHEP* **06** (2015) 119 [`arXiv:1502.07340`] [INSPIRE].

[42] S. Fichet, G. von Gersdorff, E. Pontón and R. Rosenfeld, *The Excitation of the Global Symmetry-Breaking Vacuum in Composite Higgs Models*, *JHEP* **09** (2016) 158 [`arXiv:1607.03125`] [INSPIRE].

[43] S. Fichet, G. von Gersdorff, E. Pontón and R. Rosenfeld, *The Global Higgs as a Signal for Compositeness at the LHC*, *JHEP* **01** (2017) 012 [`arXiv:1608.01995`] [INSPIRE].

[44] R.M. Schabinger and J.D. Wells, *A Minimal spontaneously broken hidden sector and its impact on Higgs boson physics at the large hadron collider*, *Phys. Rev. D* **72** (2005) 093007 [`hep-ph/0509209`] [INSPIRE].

[45] C. Carimalo, P. Kessler and J. Parisi, *On the Validity of the Equivalent Photon Approximation for Virtual Photon-Photon Collisions*, *Phys. Rev. D* **20** (1979) 1057 [INSPIRE].

[46] V.M. Budnev, I.F. Ginzburg, G.V. Meledin and V.G. Serbo, *The Two photon particle production mechanism. Physical problems. Applications. Equivalent photon approximation*, *Phys. Rept.* **15** (1975) 181 [INSPIRE].

[47] V.A. Khoze, A.D. Martin and M.G. Ryskin, *Prospects for new physics observations in diffractive processes at the LHC and Tevatron*, *Eur. Phys. J. C* **23** (2002) 311 [`hep-ph/0111078`] [INSPIRE].

[48] V.A. Khoze, A.D. Martin and M.G. Ryskin, *Photon exchange processes at hadron colliders as a probe of the dynamics of diffraction*, *Eur. Phys. J. C* **24** (2002) 459 [`hep-ph/0201301`] [INSPIRE].

[49] E. Gotsman, E. Levin, U. Maor, E. Naftali and A. Prygarin, *Survival probability of large rapidity gaps*, in *HERA and the LHC: A Workshop on the Implications of HERA for LHC Physics: CERN-DESY Workshop 2004/2005 (Midterm Meeting, CERN, 11–13 October 2004; Final Meeting, DESY, 17–21 January 2005)*, pp. 221–241, 2005 [`hep-ph/0511060`] [INSPIRE].

[50] L.A. Harland-Lang, V.A. Khoze and M.G. Ryskin, *Exclusive physics at the LHC with SuperChic 2*, *Eur. Phys. J. C* **76** (2016) 9 [`arXiv:1508.02718`] [INSPIRE].

[51] L.A. Harland-Lang, V.A. Khoze and M.G. Ryskin, *Exclusive LHC physics with heavy ions: SuperChic 3*, *Eur. Phys. J. C* **79** (2019) 39 [`arXiv:1810.06567`] [INSPIRE].

[52] D. d'Enterria and J.-P. Lansberg, *Study of Higgs boson production and its $b\bar{b}$ decay in γ-γ processes in proton-nucleus collisions at the LHC*, *Phys. Rev. D* **81** (2010) 014004 [`arXiv:0909.3047`] [INSPIRE].

[53] S. Fichet, A. Tonero and P. Rebello Teles, *Sharpening the shape analysis for higher-dimensional operator searches*, *Phys. Rev. D* **96** (2017) 036003 [`arXiv:1611.01165`] [INSPIRE].

[54] M. Boonekamp et al., *FPMC: A generator for forward physics*, arXiv:1102.2531 [InSPIRE].

[55] J. Alwall et al., *The automated computation of tree-level and next-to-leading order differential cross sections, and their matching to parton shower simulations*, *JHEP* **07** (2014) 079 [arXiv:1405.0301] [InSPIRE].

[56] M. Beneke, P. Falgari, S. Klein and C. Schwinn, *Hadronic top-quark pair production with NNLL threshold resummation*, *Nucl. Phys. B* **855** (2012) 695 [arXiv:1109.1536] [InSPIRE].

[57] T. Sjöstrand, S. Mrenna and P.Z. Skands, *A Brief Introduction to PYTHIA 8.1*, *Comput. Phys. Commun.* **178** (2008) 852 [arXiv:0710.3820] [InSPIRE].

[58] T. Gehrmann et al., W^+W^- *Production at Hadron Colliders in Next to Next to Leading Order QCD*, *Phys. Rev. Lett.* **113** (2014) 212001 [arXiv:1408.5243] [InSPIRE].

[59] CDF collaboration, *Dijet production by double Pomeron exchange at the Fermilab Tevatron*, *Phys. Rev. Lett.* **85** (2000) 4215 [InSPIRE].

[60] DELPHES 3 collaboration, *Delphes 3: a modular framework for fast simulation of a generic collider experiment*, *JHEP* **02** (2014) 057 [arXiv:1307.6346] [InSPIRE].

[61] CMS collaboration, *Performance of Electron Reconstruction and Selection with the CMS Detector in Proton-Proton Collisions at $\sqrt{s} = 8$ TeV*, 2015 *JINST* **10** P06005 [arXiv:1502.02701] [InSPIRE].

[62] CMS collaboration, *Energy Calibration and Resolution of the CMS Electromagnetic Calorimeter in pp Collisions at $\sqrt{s} = 7$ TeV*, 2013 *JINST* **8** P09009 [arXiv:1306.2016] [InSPIRE].

[63] M. Cacciari, G.P. Salam and G. Soyez, *FastJet User Manual*, *Eur. Phys. J. C* **72** (2012) 1896 [arXiv:1111.6097] [InSPIRE].

[64] M. Cacciari, G.P. Salam and G. Soyez, *The anti-k_t jet clustering algorithm*, *JHEP* **04** (2008) 063 [arXiv:0802.1189] [InSPIRE].

[65] CMS collaboration, *Identification of b-Quark Jets with the CMS Experiment*, 2013 *JINST* **8** P04013 [arXiv:1211.4462] [InSPIRE].

[66] CMS collaboration, *Description and performance of track and primary-vertex reconstruction with the CMS tracker*, 2014 *JINST* **9** P10009 [arXiv:1405.6569] [InSPIRE].